

Non-rotating convective self-aggregation in a limited area AGCM

Nathan P. Arnold^{1,2}, William M. Putman²

¹Goddard Earth Sciences Technology and Research, Universities Space Research Association, Columbia, Maryland

²Global Modeling and Assimilation Office, NASA Goddard Space Flight Center, Greenbelt, Maryland

Key Points:

- The sensitivity of parameterized convection to mid-tropospheric humidity enhances aggregation.
- Humid clusters have a maximum scale of 3-4000 km, limited by the boundary layer momentum balance.
- Larger clusters have warmer humid-region boundary layers and deeper convective heating.

Corresponding author: Nathan Arnold, nathan.arnold@nasa.gov

Abstract

We present non-rotating simulations with the Goddard Earth Observing System (GEOS) atmospheric general circulation model (AGCM) in a square limited area domain over uniform sea surface temperature. As in previous studies, convection spontaneously aggregates into humid clusters, driven by a combination of radiative and moisture-convective feedbacks. The aggregation is qualitatively independent of resolution, with horizontal grid spacing from 3 km to 110 km, with both explicit and parameterized deep convection. A budget for the spatial variance of column moist static energy suggests that longwave radiative and surface flux feedbacks help establish aggregation, while the shortwave feedback contributes to its maintenance. Mechanism denial experiments confirm that aggregation does not occur without interactive longwave radiation. Ice cloud radiative effects help support the humid convecting regions, but are not essential for aggregation, while liquid clouds have a negligible effect. Removing the dependence of parameterized convection on tropospheric humidity reduces the intensity of aggregation, but does not prevent the formation of dry regions. In domain sizes less than $(5000 \text{ km})^2$, the aggregation takes the form of a single cluster, while larger domains develop multiple clusters. Larger domains initialized with a single large cluster are unable to maintain them, suggesting an upper size limit. Surface windspeed increases with domain size, implying that maintenance of the boundary layer momentum balance may limit cluster size. As cluster size increases, large boundary layer temperature anomalies develop to maintain the surface pressure gradient, leading to an increase in the depth of parameterized convective heating and an increase in gross moist stability.

1 Introduction

A growing number of numerical models have now simulated an instability in idealized radiative convective equilibrium (RCE), in which deep convection “self-aggregates” into humid clusters, even in the absence of inhomogeneities in boundary conditions and forcing. This instability occurs in 2D and 3D domains, with and without rotation, in non-hydrostatic cloud resolving models (CRMs) and general circulation models (GCMs) with parameterized convection.

The phenomenon is of interest for a variety of reasons. The idealized non-rotating RCE framework allows for the study of feedbacks in a simplified context, and may be useful as a platform for model development, allowing for quick inter-comparisons of model

44 physics [*Wing et al.*, 2017b]. A better understanding of the aggregation process may pro-
45 vide insight into observed phenomena, such as tropical cyclones [*Wing et al.*, 2016] or the
46 Madden-Julian Oscillation (MJO) [*Arnold and Randall*, 2015], although it remains unclear
47 to what extent the lessons of aggregation apply to the real world. *Wing et al.* [2017] and *Hol-*
48 *loway and Woolnough* [2016] present excellent reviews of previous work on aggregation; we
49 will provide only a brief overview here.

50 Aggregation typically begins with the formation of a dry patch, driven by radiative
51 cooling and subsidence, in which convection is suppressed [*Emanuel et al.*, 2014]. This dry
52 patch expands while convection and rainfall intensify elsewhere in the domain, eventually
53 becoming confined to a humid region covering roughly 20-25% of the domain area. Aggre-
54 gation is usually accompanied by a decrease in domain mean humidity, and an increase in
55 outgoing longwave radiation (OLR). In concentrating the same amount of precipitation in a
56 smaller, more humid area, the effects of convective entrainment are minimized, precipitation
57 efficiency is increased, and the free troposphere becomes warmer and drier than when con-
58 vection is scattered. Observations show a correlation between the degree of cloud organiza-
59 tion, reduced humidity, and enhanced OLR [*Tobin et al.*, 2012, 2013], suggesting that some
60 aspects of idealized aggregation are relevant to the real world. *Stein et al.* [2017] found that,
61 in CloudSat-CALIPSO data, the vertical distribution of cloud fraction shifts with the degree
62 of aggregation, with a decrease in high cloud fraction and increases in low cloud.

63 The transition to aggregation is primarily driven by diabatic feedbacks, although the
64 details appear to depend on the model physics and boundary conditions. Many studies have
65 found that aggregation will not occur when radiation is made non-interactive [*Bretherton*
66 *et al.*, 2005; *Muller and Held*, 2012; *Holloway and Woolnough*, 2016], but there is disagree-
67 ment over the role of high [*Bretherton et al.*, 2005; *Stephens et al.*, 2008] versus low cloud
68 [*Muller and Held*, 2012], and clear-sky effects [*Emanuel et al.*, 2014]. Surface fluxes and
69 shortwave radiation can impact aggregation [*Wing and Cronin*, 2016; *Wing and Emanuel*,
70 2014], but in most cases are not essential. The resolved transport of moist static energy is
71 generally down-gradient, acting to reduce the spatial variance of humidity and therefore op-
72 posing aggregation [*Wing and Emanuel*, 2014; *Holloway and Woolnough*, 2016]; in equilib-
73 rium, this is the primary “negative feedback” balancing diabatic input to the humid region.
74 Rain re-evaporation and the formation of cold pools can also oppose aggregation [*Muller*
75 *and Bony*, 2015], and contributes to a dependence on model domain size [*Jeevanjee and*

76 *Romps*, 2013]. The relative importance of each of these processes varies over time *Wing and*
77 *Emanuel* [2014]; *Holloway and Woolnough* [2016].

78 There are several examples in the literature of aggregation occurring more readily or
79 more intensely with higher surface temperatures [*Khairoutdinov and Emanuel*, 2010; *Wing*
80 *and Emanuel*, 2014; *Emanuel et al.*, 2014; *Coppin and Bony*, 2015], although aggregation
81 has also been found over low SST [*Abbot*, 2014; *Holloway and Woolnough*, 2016; *Wing and*
82 *Cronin*, 2016]. This possible temperature dependence, combined with the typical reduction
83 in mean humidity and increased OLR accompanying an aggregated state, has led to the sug-
84 gession that aggregation could serve as a tropical thermostat [*Khairoutdinov and Emanuel*,
85 2010; *Mauritsen and Stevens*, 2015; *Bony et al.*, 2016].

86 There has also been interest in the factors controlling the length scale of aggregation.
87 In cloud resolving models, typical domains are small enough that only a single convective
88 cluster emerges, although elongated channel domains have developed multiple clusters [*Wing*
89 *and Cronin*, 2016]. Aggregation develops more readily in large domains, and generally does
90 not occur at all below a certain domain size, although this lower limit is relaxed when low-
91 level re-evaporation is switched off [*Muller and Bony*, 2015; *Holloway and Woolnough*,
92 2016]. This implies that aggregation has a preferred length scale larger than the typical CRM
93 domain size. Simulations of RCE in global models have formed both singular and multiple
94 clusters on a range of scales [*Held et al.*, 2007; *Reed et al.*, 2015; *Arnold and Randall*, 2015;
95 *Coppin and Bony*, 2015; *Silvers et al.*, 2016]. The physical processes controlling the quan-
96 tity and scale of aggregated clusters are poorly understand, although mechanisms have been
97 proposed [*Wing and Cronin*, 2016; *Yang*, 2017]. The answers could be relevant for theoret-
98 ical studies of the MJO, in which scale selection remains an important open question [*Kuang*,
99 2011; *Adames and Kim*, 2016].

100 This paper is motivated by a lack of consensus on several key questions. First, is a de-
101 pendence on free tropospheric humidity important to the clustering of convection, or are con-
102 vection and humidity independently organized by the large-scale flow? This question can
103 be difficult to probe in a cloud resolving model, where there is no intrinsic separation be-
104 tween convection and large-scale motion. Here we use parameterized convection, which can
105 be more easily manipulated, to show that moisture-convection feedbacks enhance aggrega-
106 tion, but are not essential to it. Second, is there an upper limit to the convective cluster size,
107 and what physical processes set that limit? We show that convection begins to form multi-

108 ple clusters in domains larger than a critical size, and suggest this is due to the difficulty of
109 maintaining the boundary layer flow of a single large cluster against dissipation.

110 A third question is whether there is any fundamental distinction between the aggrega-
111 tion seen in CRMs, and that seen in models with parameterized convection? Aggregation has
112 been studied in both cloud resolving models with relatively high resolution ($dx < 5$ km) and
113 general circulation models with parameterized clouds and convection ($dx \approx 100$ km). One
114 goal of this study is to bridge these two regimes, both in resolution and domain geometry.
115 Here we use the atmospheric component of the NASA Goddard Earth Observing System
116 (GEOS), a model somewhat unique in that it is a global AGCM with the ability to run in a
117 CRM-like doubly periodic domain. The model is routinely run across a wide range of hori-
118 zontal resolutions (discussed below), with physical parameterizations designed to adapt with
119 the grid spacing. We find no qualitative difference between aggregation with explicit convec-
120 tion ($dx \approx 3$ km) and parameterized convection ($dx \approx 100$ km).

121 The GEOS model and experimental setup are described in section 2. Section 3 presents
122 a reference case of non-rotating aggregation. We explore the dependence of aggregation on
123 model resolution in section 4, and the domain size dependence in section 5. A mechanism
124 limiting the spatial scale of aggregated clusters is proposed in section 6, and section 7 con-
125 cludes with a summary and discussion of our findings.

126 **2 Model description**

127 The Goddard Earth Observing System (GEOS) is an atmosphere-ocean general circula-
128 tion model (AOGCM) developed by the NASA Global Modeling and Assimilation Office
129 (GMAO) [Molod *et al.*, 2012]. GEOS is used in a variety of applications, including daily
130 production of short range weather forecasts for NASA mission support, production of the
131 Modern Era Reanalysis for Research and Applications [Rienecker *et al.*, 2011; Bosilovich,
132 *et al.*, 2015], global mesoscale simulations [Putman and Suarez, 2011; Putman *et al.*, 2014],
133 and basic research in atmospheric chemistry, stratospheric dynamics and other topics. Model
134 grid spacing ranges from roughly 50 km for MERRA-2 production to 7 km in global mesoscale
135 runs. Configured as a coupled system, the model is used for seasonal prediction [Ham *et al.*,
136 2014], and decadal climate projections were submitted to the Coupled Model Intercompari- son
137 Project (CMIP-5) [Ham *et al.*, 2014].

138 Here we use the atmospheric component of GEOS, based on the FV3 finite volume
139 dynamical core [Putman and Lin, 2007]. Convection is parameterized with the Relaxed
140 Arakawa-Schubert (RAS) scheme of Moorthi and Suarez [1992]. Boundary layer turbulence
141 is based on a combination of the Lock *et al.* [2000] scheme of non-local mixing in unstable
142 layers, and the Richardson number-based scheme of Louis *et al.* [1982] in stable conditions.
143 Shortwave radiation follows Chou [1990] and Chou [1992] and longwave radiation is taken
144 from Chou and Suarez [1994]. The model uses a prognostic cloud fraction, liquid and ice
145 scheme described in Bacmeister *et al.* [2006]. All simulations presented here use single mo-
146 ment microphysics.

147 Resolution dependence appears in the model physics through the width of the prob-
148 ability density function governing large-scale cloud fraction, the physics timestep, and in
149 constraints on RAS. As in the default model, a stochastic Tokioka parameter [Tokioka *et al.*,
150 1988] is used to convert the RAS scheme to a shallow non-precipitating scheme at high res-
151 olution. The entrainment rate is subjected to a random lower limit, shifted to higher values
152 with increasing resolution. In this way, parameterized deep convection is increasingly sup-
153 pressed as resolved vertical motions become more capable of representing convective storms,
154 similar to the behavior of a scale-aware parameterization [e.g., Grell and Freitas, 2013].

155 In this study we take advantage of a new doubly periodic configuration, in which the
156 full AGCM is run on a square cartesian domain with re-entrant boundary conditions. The
157 domain and horizontal grid spacing can be set to arbitrary size, allowing for rapid testing and
158 model development. We expect this configuration to become increasingly useful as global
159 atmospheric models begin routinely operating in the “gray zone,” where convection is not yet
160 explicitly resolved, but traditional scale-separation assumptions break down [e.g., Molinari
161 and Dudek, 1992]. Single column models (SCM) are currently used in model development as
162 a platform for rapid parameterization testing, but these are unsuitable for use at high reso-
163 lutions where many parameterizations are designed to cede ground to resolved dynamics. By
164 running the full dynamics in an arbitrarily small domain, the doubly periodic configuration
165 enables parameterization testing at high resolutions with enormous computational savings
166 compared with a global run.

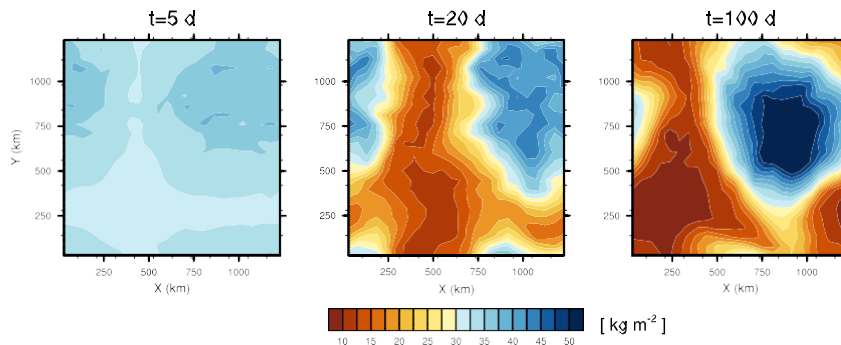
167 In all simulations presented here, sea surface temperature is fixed at 301 K. Insolation
168 has been set equal to the March 21 equatorial daily mean by fixing the zenith angle at 52.5°
169 and reducing the solar constant to 733 Wm^{-2} . Except where otherwise noted, the domains

170 are initialized with horizontally uniform conditions, based on an equilibrium profile taken
 171 from a doubly periodic run with the same SST, 25 km grid spacing, and a 100 km × 100 km
 172 domain. A white noise perturbation $O(0.1 \text{ K})$ is added to the lowest level initial temperature
 173 to break symmetry. The model is run with 72 levels, with approximately eight in the bound-
 174 ary layer. The Coriolis parameter is set to zero.

175 3 A reference case of aggregation

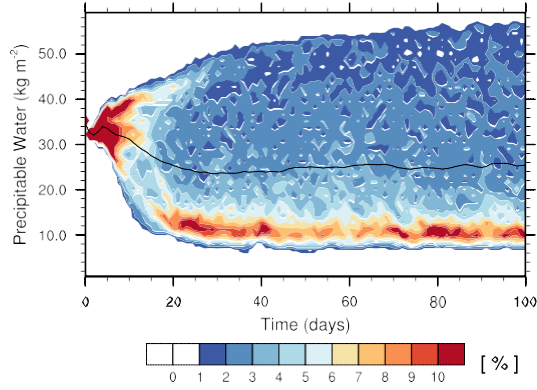
176 We begin with analysis of a representative case, in a domain 1320 km × 1320 km, with
 177 55 km horizontal grid spacing. This is a larger domain than has been used in most CRM ag-
 178 gregation studies, and at this horizontal resolution the parameterized deep convection plays
 179 an important role in removing column instability.

180 As in previous studies, the aggregation process begins with formation of a dry patch,
 181 visible by day five in the lower left of the domain (Fig. 1). Over the next two weeks the dry
 182 patch expands and becomes drier, while the remaining humid region consolidates and be-
 183 comes more humid. By day 100 the system has reached a statistical equilibrium, with a
 184 quasi-circular humid region nearly saturated in its core. The aggregation process is reflected
 185 in the evolution of the probability distribution of column water vapor (CWV) shown in Fig. 2.
 186 There is a rapid initial increase in the number of very dry columns, and a more gradual moist-
 187 ening of the humid region. The final equilibrium has high variance with a strongly skewed
 188



189 **Figure 1.** Snapshots of column water vapor on days 5, 20 and 100, for a reference case with 55 km grid
 190 spacing.

193 To understand the feedbacks responsible for aggregation we construct a budget for the
 194 variance of the column moist static energy, following *Wing and Emanuel* [2014]. Aggre-



191 **Figure 2.** The frequency distribution of column water vapor over time, for a reference case with 55 km grid
 192 spacing. Shading indicates relative percentage of AGCM columns in bins of 2 kg m^{-2} width.

195 agation is in some sense defined by large regional differences in column moist static energy
 196 (MSE), and larger spatial MSE variance is indicative of more intense aggregation. Processes
 197 that contribute to MSE variance can be thought of as causing or supporting aggregation,
 198 while processes that reduce MSE anomalies oppose aggregation.

199 We use the frozen moist static energy, h , defined

$$h = c_p T + gz + L_v q_v - L_i q_i, \quad (1)$$

200 where c_p is the specific heat capacity of air, T is temperature, g is the gravitational accelera-
 201 tion, z is height above the surface, L_v is the latent heat of vaporization, q_v is the specific hu-
 202 midity, L_i is the latent heat of fusion, and q_i is the specific ice content. Column MSE anom-
 203 alies vary according to

$$\partial_t \bar{h}^t = \bar{\omega} \partial_p \bar{h}^t + \bar{w} \cdot \nabla \bar{h}^t + \bar{W}^t + \bar{S}W^t + LHF^t + SHF^t, \quad (2)$$

204 where primes denote anomalies relative to the spatial mean, $A^t = A - \bar{A}$, and hats denote
 205 the mass-weighted column integral $\hat{A} = \int_{ps}^{pt} A dp/g$. The advection terms are calculated
 206 using instantaneous 3-hourly output, and column radiative heating is calculated from the dif-
 207 ference in fluxes between model surface and model top. All column-integrated budget terms
 208 are averaged to a daily 110 km grid before proceeding.

209 We arrive at an equation for the variance by multiplying each term in Eqn. 2 by \bar{h}^t , and
 210 normalizing by the instantaneous spatial variance, $[\bar{h}^{t2}]$, with square brackets indicating the

211 spatial mean,

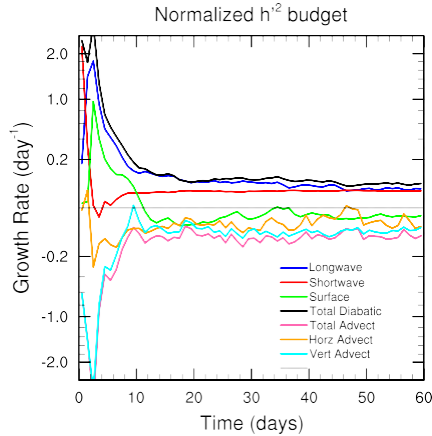
$$\frac{1}{2} \frac{\partial \overline{h^2}}{[\overline{h^2}]} = \frac{\omega \overline{c_p h^t}}{[\overline{h^2}]} + \frac{\overline{\mathbf{w} \cdot \nabla h^t}}{[\overline{h^2}]} + \frac{\overline{LW^t h^t}}{[\overline{h^2}]} + \frac{\overline{SW^t h^t}}{[\overline{h^2}]} + \frac{\overline{LHF^t h^t}}{[\overline{h^2}]} + \frac{\overline{SHF^t h^t}}{[\overline{h^2}]} \quad (3)$$

212 Taking the spatial average of Eqn. 3 yields the fractional growth rate of MSE variance
 213 attributable to each budget term. Terms in Eqn. 2 which are positively correlated with MSE
 214 anomalies, i.e., increasing MSE in regions of high MSE, or removing MSE from regions
 215 of low MSE, will add to the variance. This may be thought of as a variant of the projection
 216 method of *Andersen and Kuang* [2012], used to study convective feedbacks in the MJO [e.g.,
 217 *Arnold et al.*, 2013, 2015], here applied to instantaneous anomalies rather than composites to
 218 allow a time-varying quantification of feedback processes.

219 The fractional growth rates defined by the spatial average of Eqn. 3 are shown in Fig. 3.
 220 We utilize the color scheme of *Wing and Emanuel* [2014] and *Holloway and Woolnough*
 221 [2016] to allow easy comparison. As in those studies, the diabatic terms - radiation and sur-
 222 face fluxes - appear to be the early drivers of aggregation. The longwave feedback dominates
 223 over the first 30 days, gradually diminishing until it is similar to the shortwave contribution.
 224 Surface fluxes strongly amplify MSE variance over the first 10 days, and then become weakly
 225 damping. Contributions from horizontal and vertical advection are consistently negative, and
 226 of comparable magnitude over most of the simulation.

227 This evolution is similar to the control case of *Holloway and Woolnough* [2016], al-
 228 though we find larger initial growth rates during the first five days of the simulation, and
 229 a large initial damping effect from vertical advection not seen in their study. These differ-
 230 ences may be related. If vertical advection initially offsets growth from the diabatic terms,
 231 the MSE variance would grow more slowly and maintain a small denominator in Eqn. 3. The
 232 advection difference may stem from the grid spacing (4 km versus 55 km) or the use of a
 233 non-hydrostatic instead of hydrostatic dynamical core. There are somewhat larger differences
 234 relative to *Wing and Emanuel* [2014], who found an intermediate stage of aggregation in
 235 which the contribution from advection is temporarily positive. Despite this, the final equilib-
 236 ria are similar, though longwave heating remains more important than shortwave throughout
 237 our simulation.

241 Additional insight can be gained from the spatial pattern of feedbacks. We sort the
 242 budget terms of Eqn. 2 by the column water vapor (CWV) and plot them in moisture-time
 243 space to provide a sense of how the growth rates of Fig. 3 are arrived at. As expected, col-

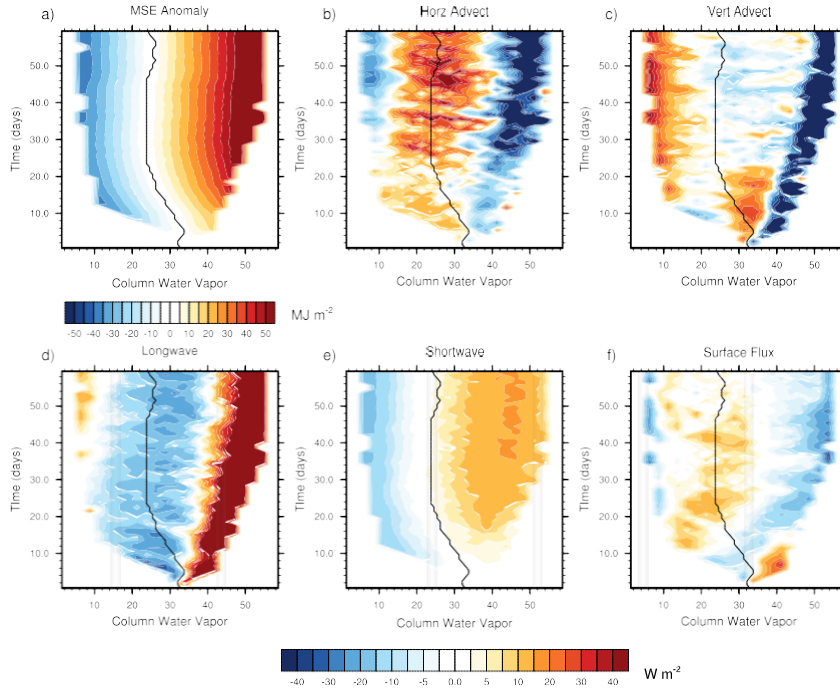


238 **Figure 3.** Fractional growth rate of MSE spatial variance due to each budget term. Radiative terms gener-
 239 ally contribute to MSE variance, while advection reduces it. The contribution from surface fluxes is initially
 240 positive but becomes negative as convection is organized. Note non-linear vertical axis.

244 umn moist static energy anomalies (Fig. 4a) vary almost monotonically with CWV. A single
 245 black contour indicates the column water bin corresponding to the domain-mean MSE, i.e.,
 246 an MSE anomaly of zero. As seen in the column water PDF of Fig. 2, domain-mean column
 247 water decreases by roughly 10 kg m^{-2} as aggregation develops.

248 Budget terms with positive anomalies (red shading) to the right of the zero line, or neg-
 249 ative anomalies (blue shading) to the left, will tend to increase MSE spatial variance. It is ap-
 250 parent that most processes contribute a mixture of amplifying and damping MSE anomalies
 251 at different points in the model domain. The single exception is shortwave radiation, which
 252 amplifies MSE anomalies everywhere. Anomalies in horizontal and vertical advection are
 253 both strongly negative in the most humid columns, but their combination is positive in the
 254 moderately humid regions, amplifying anomalies there. Their sum is also positive across the
 255 dry regions. The longwave anomalies are strongly positive in the humid columns, balancing
 256 the advection, and negative over the regions of moderate humidity. Surface fluxes offer the
 257 weakest feedback, which is generally negative after day 10.

260 Many studies of aggregation have identified a shallow circulation between dry and hu-
 261 mid regions which transports MSE up-gradient, maintaining the aggregated state [Brether-
 262 ton et al., 2005; Muller and Held, 2012; Muller and Bony, 2015; Holloway and Woolnough,
 263 2016]. The circulation is thought to be driven by low-level radiative cooling anomalies in
 264 the dry regions; with little convection in these regions, radiative cooling is almost entirely



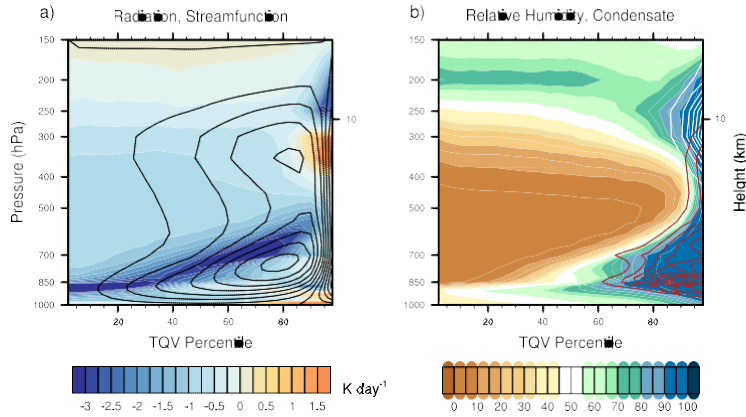
258 **Figure 4.** (a) Column MSE anomalies binned by column water vapor. (b-f) Anomalous MSE tendencies
 259 due to horizontal and vertical advection, longwave and shortwave radiative heating, and surface enthalpy flux.

265 balanced by subsidence-driven adiabatic warming. The source of these radiative cooling
 266 anomalies - low clouds or clear-sky humidity gradients - appears to depend on the model
 267 used.

268 Based on the isobaric continuity equation, an effective stream function $\Psi_i(p)$ repre-
 269 senting flow across column moisture space, may be defined,

$$\Psi_i(p) = \Psi_{i-1}(p) + \omega_i(p) \quad (4)$$

270 where ω_i is the mean pressure velocity in the i -th CWV bin. Note this differs slightly from
 271 the mass flux streamfunction derived by *Bretherton et al.* [2005], though the two result in
 272 qualitatively similar circulations. This stream function is shown in Fig. 5a (black contours),
 273 along with CWV-binned total radiative cooling. The plot makes clear that the regions of
 274 strongest descent coincide with the strongest radiative cooling rates. Figure 5b shows binned
 275 profiles of relative humidity (shading) and cloud liquid and ice condensate (red and white
 276 contours). Low cloud cover is minimal in the dry regions, but a sharp vertical gradient in
 277 humidity is seen, which appears to be the primary factor in low-level radiative cooling.



278 **Figure 5.** (a) Radiative cooling profiles as a function of column water vapor (shading), and stream function
 279 representing flow between dry and humid regions (contours). (b) Relative humidity (shading) and cloud ice
 280 and liquid condensate (white and red contours). Condensate contours begin at 0.01 kg kg^{-1} with 0.0125 kg
 281 kg^{-1} intervals.

282 Several studies have shown that the aggregation process can be prevented by homoge-
 283 nizing radiative heating, or by removing the effects of different cloud types on radiative heat-
 284 ing [Bretherton *et al.*, 2005; Muller and Held, 2012; Arnold *et al.*, 2015]. Here we conduct
 285 similar “mechanism denial” experiments to understand processes important to aggregation.

286 First, the longwave radiative heating is made horizontally uniform. The longwave
 287 fluxes in each column are calculated normally, but the heating tendencies are horizontally
 288 averaged over the domain before being applied. The local radiative feedback is therefore re-
 289 moved, while leaving a domain mean feedback intact. The column water vapor on day 120
 290 of this simulation is shown in Fig. 6a, with a mean value roughly 10 kg m^{-2} higher than the
 291 reference case (Table 1). The striking uniformity of water vapor in the domain confirms the
 292 importance of longwave feedbacks to the simulated aggregation.

293 *Muller and Bony* [2015] and *Holloway and Woolnough* [2016] found that aggregation
 294 could still occur in a CRM with homogenized radiation, so long as cold pool formation was
 295 inhibited by switching off rain re-evaporation in the lowest 1.5 km. *Muller and Bony* [2015]
 296 suggested that a “moisture-memory” feedback was responsible for the aggregation, in which
 297 convection preferentially develops in regions of high humidity. Their experiment, and re-
 298 lated work by *Jeevanjee and Romps* [2013], imply that cold pools are important in inhibiting
 299 aggregation in CRMs. In the experiment shown here with 55 km grid spacing, cold pools
 300 remain unresolved and are not explicitly parameterized. Although the model does include re-

301 evaporation of rain, the RAS convection scheme includes no explicit downdrafts. In a related
302 test (not shown), we switched off rain re-evaporation while the longwave heating tendency
303 was homogenized over the domain, mimicking the experiment of *Muller and Bony* [2015].
304 This resulted in a lower domain mean humidity, but no increase in organization after 90 days.
305 This suggests that either the “moisture-memory” feedback is relatively weak in this model, or
306 there are additional processes acting to inhibit aggregation.

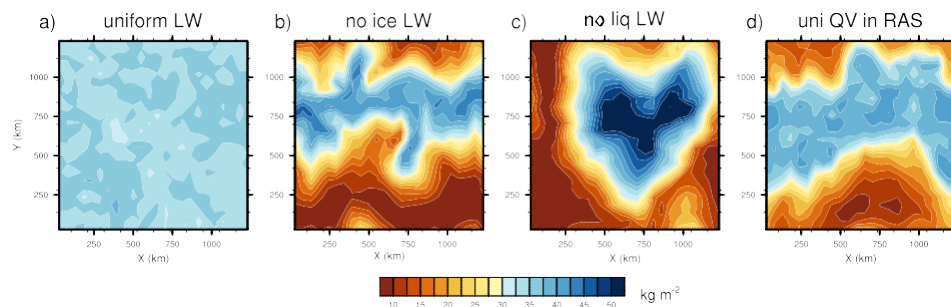
307 We can isolate the importance of clouds to the longwave feedback by selectively set-
308 ting to zero the liquid or ice condensate in the model’s longwave radiative code. Eliminat-
309 ing the ice cloud radiative effect results in a moderately humid band of convection (Fig. 6b).
310 While the dry anomalies are similar to those of the reference case, the humid regions are
311 less humid and apparently unable to form a compact cluster. The implication is that the ice
312 cloud radiative effect plays a role in supporting the region of deep convection (where such
313 clouds principally occur) but contributes little to the formation and maintenance of dry re-
314 gions. *Holloway and Woolnough* [2016] made a geometric argument for the occurrence of
315 banded versus circular humid regions which may apply here: supposing that the convecting
316 regions tend to minimize their perimeter-to-area ratio, convection will form a banded struc-
317 ture in a square domain when the required convecting area exceeds L^2/π , with L the domain
318 length. Ice cloud radiative effects may intensify ascent in the humid region and reduce the
319 area required for convection, allowing for a compact circular patch. When this feedback is
320 removed, the less intense convection requires a larger area to balance radiative cooling across
321 the domain, and takes on a banded structure to minimize its perimeter.

322 Eliminating the radiative effect of shallow liquid clouds (Fig. 6c) has less effect on the
323 aggregation, with no obvious differences relative to the reference case. This contrasts with
324 *Muller and Held* [2012], who found that radiative cooling associated with liquid clouds was
325 essential to driving the shallow circulation that maintained aggregation. As suggested above,
326 the low-level radiative cooling here is primarily a clear-sky effect, due to the sharp humidity
327 gradient at the top of the boundary layer.

328 Finally, we consider the role of convection-moisture interaction. Until recently, there
329 had been little direct evidence that the interaction between convection and tropospheric hu-
330 midity plays a role in aggregation. *Tompkins and Semie* [2017] found a significant impact
331 from the choice of sub-grid mixing scheme in a CRM, with schemes that produced enhanced
332 mixing around updraft cores also producing stronger aggregation, implying that convective

333 entrainment processes are important. Here we conduct an analogous experiment in a model
 334 with parameterized convection, where it is possible to homogenize the humidity field “seen”
 335 by the parameterization without actually altering the humidity. We horizontally average the
 336 free tropospheric ($p < 850$ hPa) water vapor passed to the Relaxed Arakawa Schubert (RAS)
 337 scheme; the parameterized convection then behaves as though the same humidity profile is
 338 present throughout the domain, while the radiative and resolved dynamical effects of mois-
 339 ture variability are preserved. The result is shown in Fig. 6d. Aggregation is weaker, with
 340 convection again occupying a band of moderate humidity, with less spatial moisture variance
 341 than any experiment except that with homogenized longwave radiation.

342 This reduction in aggregation intensity is consistent with moisture mode theories [*So-*
 343 *bel et al., 2001; Fuchs and Raymond, 2005; Sobel and Maloney, 2012*], wherein deep con-
 344 vection, modulated by turbulent entrainment, is assumed to be a function of tropospheric
 345 humidity. Such a causal relationship has been seen in CRM experiments [*Derbyshire et al.,*
 346 *2004*], and a strong correlation between column humidity and precipitation is seen in nature
 347 [*Bretherton et al., 2005*]. On the other hand, in this model the modulation of convection by
 348 humidity is clearly secondary in importance to the radiative feedbacks. It is possible that the
 349 relatively small impact here may result from insufficient moisture sensitivity in RAS, or from
 350 a large fraction of the total precipitation being generated by large-scale condensation rather
 351 than parameterized convection.



352 **Figure 6.** Snapshots of column water vapor in mechanism denial experiments at equilibrium. (a) Horizont-
 353 tally uniform longwave heating, (b) no cloud ice radiative effect, (c) no cloud liquid radiative effect, and (d)
 354 uniform water vapor seen by the RAS convection scheme.

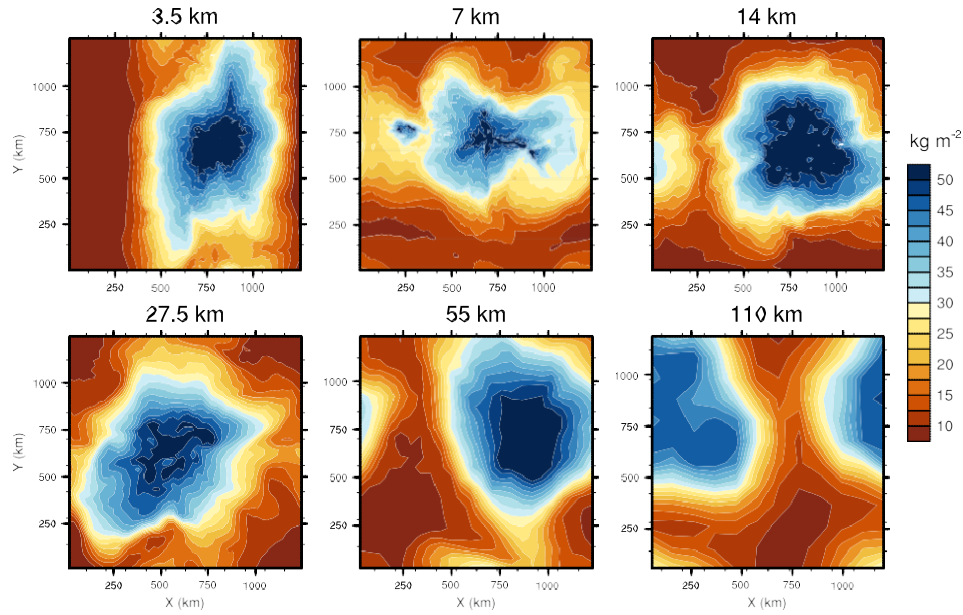
355 **4 The resolution dependence of aggregation**

356 To more directly connect the aggregation described above with that seen in cloud res-
357 solving model simulations, we conduct a series of experiments with decreasing grid spacing.
358 The GEOS model physics are designed to adapt with horizontal resolution, allowing appli-
359 cations with grid spacing from 3 km to 110 km. Here we consider the sensitivity of aggre-
360 gation to grid spacing across this range. The boundary conditions and domain size for all
361 experiments are identical to the reference case described above.

362 We find that aggregation develops in every case, though with some quantitative differ-
363 ences. Snapshots of column water vapor (CWV) in the equilibrated simulations are shown
364 in Fig. 7. The convective clusters are most humid with 14 km and 55 km grid spacing. The
365 clusters are generally circular, although the 3.5 km case is nearly banded. There is some
366 variability in the drier part of the “band,” but the structure is essentially stable over the last
367 40 days of the simulation. Dry regions are less dry in the 7 km case, which also exhibits a
368 smaller and irregularly shaped humid region. This case is firmly in the “gray zone,” where
369 convective motions remain only partially resolved, and the present balance between resolved
370 and parameterized convection may require adjustment. We note that coarsening the high res-
371 olution fields to a common 110 km grid has no qualitative effect on the aggregation’s appear-
372 ance.

375 The vertical structures of the radiative cooling and humid-dry circulations also remain
376 similar. Figure 8 shows the profiles of radiative cooling binned by column water vapor and
377 the inter-CWV stream function for each experiment. There is some variation in the strength
378 of radiative cooling with resolution, e.g., between the 3 km and 55 km cases, which raises the
379 possibility of resolution dependence in the radiative feedbacks discussed in Section 3. De-
380 spite the differences in radiative cooling, the circulation varies little with resolution, although
381 it is slightly weaker in the 3 km case, and stronger in the 55 km. There is also a slight deep-
382 ening of the ascent profiles in the humid region at coarser resolutions. This may be a conse-
383 quence of the increasing Tokioka restriction on RAS, which limits the depth of convective
384 heating at high resolutions. Figure 9 shows binned profiles of the parameterized convective
385 mass flux, indicating that convective depth generally decreases with resolution as expected.

386 Some studies have found qualitative changes with model resolution. *Muller and Held*
387 [2012] showed that aggregation in a CRM no longer developed from a disaggregated state
388 when grid spacing was reduced from 2 km to 1 km, and *Reed and Medeiros* [2016] found

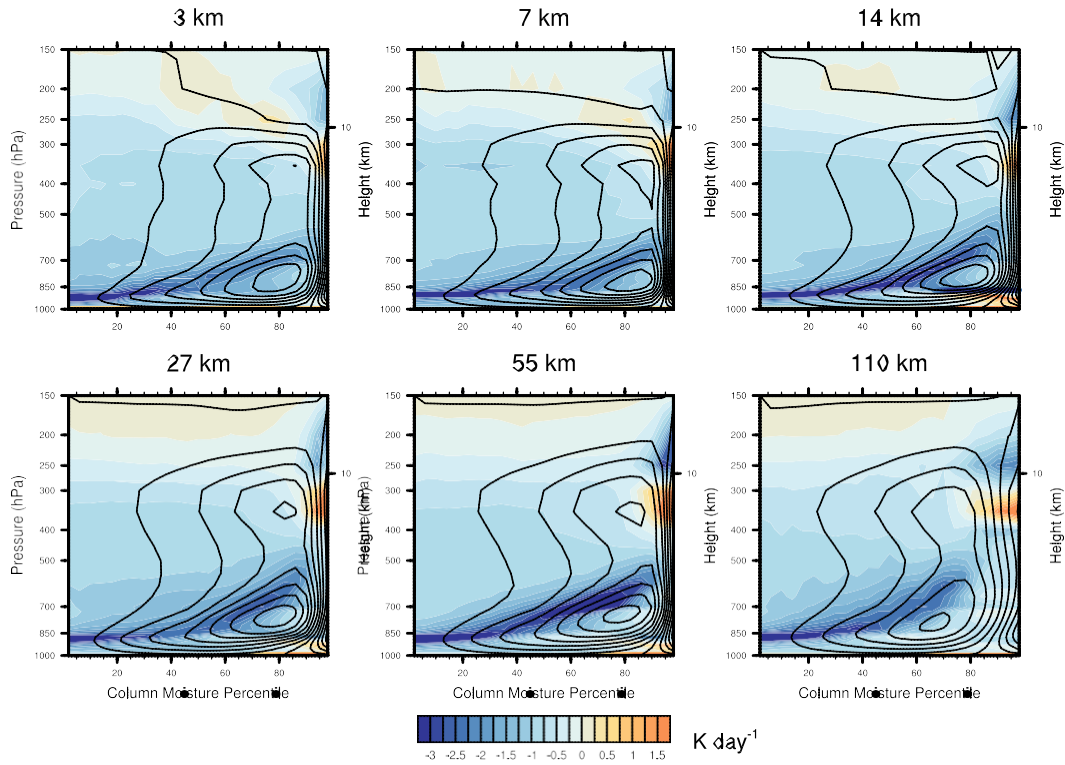


373 **Figure 7.** Snapshots of column water vapor on day 120 of simulations with 1320 km domain, and grid
 374 spacing varying from 3.5 km to 110 km.

389 that the intensity of aggregation in an AGCM significantly increased as the grid spacing was
 390 reduced from 110 km to 7 km, with a similar reduction in planetary radius. It is possible the
 391 relative insensitivity to resolution seen here results from the GEOS model physics, which
 392 have been carefully tuned at multiple resolutions. However, we did not run with grid spacing
 393 less than 3 km, nor in a spherical Earth-sized domain, so we cannot rule out qualitatively
 394 different behavior in those regimes.

399 **5 The domain size dependence of aggregation**

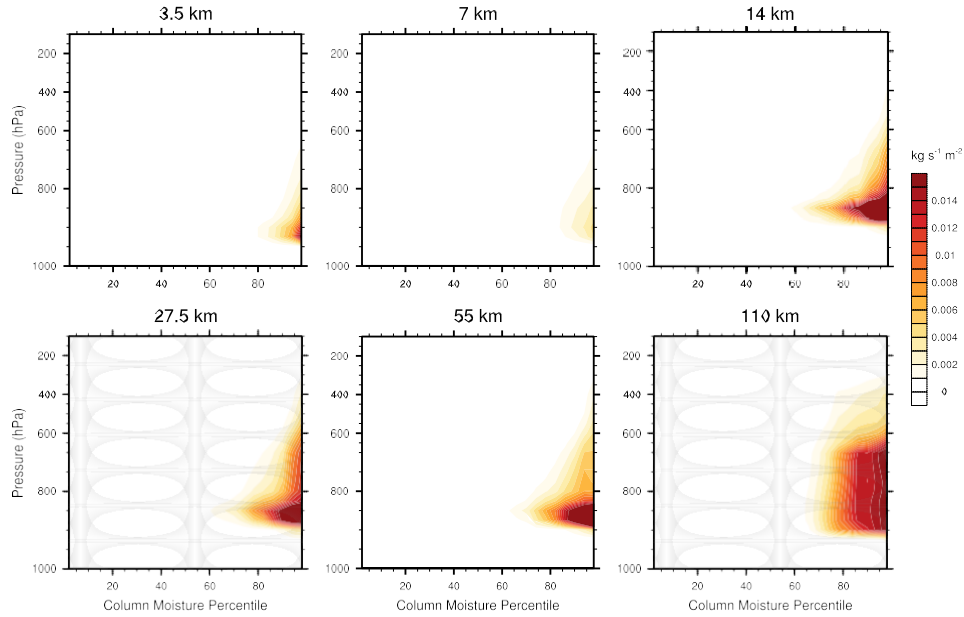
400 In this section we increase the domain size to examine how aggregation changes with
 401 horizontal scale. *Muller and Held* [2012] and *Silvers et al.* [2016] both found some domain
 402 size dependence of aggregation, the former using a CRM with square domains approxi-
 403 mately 100 km to 500 km, and the latter using an AGCM with square domains from 800 km
 404 to 13000 km. Muller and Held found that convection would aggregate into quasi-circular
 405 clusters in domains larger than 200 km, but convection remained disorganized in smaller do-
 406 mains, a constraint that may be related to cold pool formation [*Jeevanjee and Romps*, 2013].
 407 Silvers et al. found a linear form of organized convection in their larger domains, while the
 408 smallest domain appeared unable to capture the same level of organization.



395 **Figure 8.** Profiles of radiative cooling (shading) and stream functions representing flow between dry and
 396 humid regions (contours), in simulations with varying grid spacing.

409 Here we run with domain edges of 1320 km, 2640 km, 4950 km, and 9900 km. All
 410 simulations use 55 km grid spacing. Snapshots of column water vapor are shown in Fig. 10,
 411 on days 120, 150, and 180 for the 1320 km, 2640 km, and 4950 km cases, and day 300 for the
 412 9900 km case. We use later snapshots for the larger domains because they take somewhat
 413 longer to equilibrate. The three smaller domains all show a single circular humid cluster.
 414 The domain-mean water vapor increases with domain size (Table 1), but the three cases are
 415 otherwise quite similar. The 9900 km case is unique in developing multiple clusters, with
 416 five distinct humid regions visible on day 300. There is considerable variability in the cluster
 417 configuration, with clusters alternately merging and breaking apart, but the two large clusters
 418 seen in Fig. 10 are representative of the maximum size seen, suggesting an upper scale limit
 419 of roughly 4000 km.

422 To assess whether the multiple clusters might eventually merge, given sufficient time,
 423 we initialized the 9900 km domain with a single humid cluster, using state fields from the
 424 4950 km case at equilibrium and linearly interpolated to match the larger domain. Figure 11

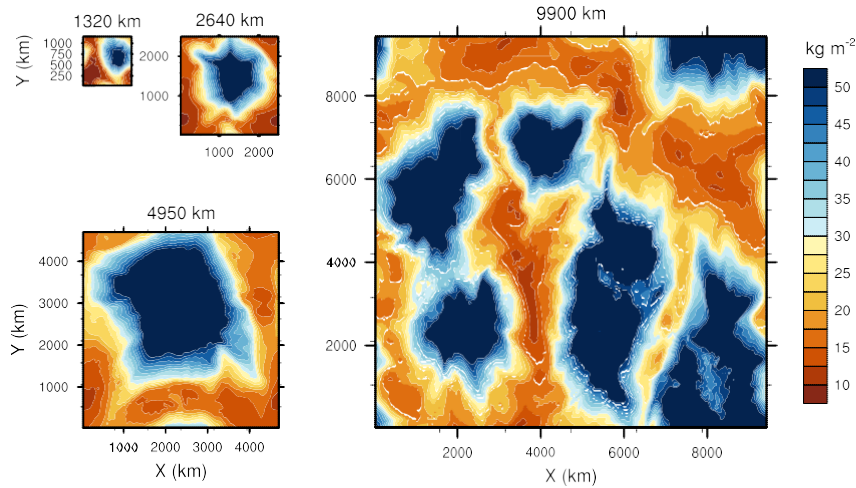


397 **Figure 9.** Profiles of parameterized convective mass flux, binned by column water vapor, in simulations
 398 with varying grid spacing.

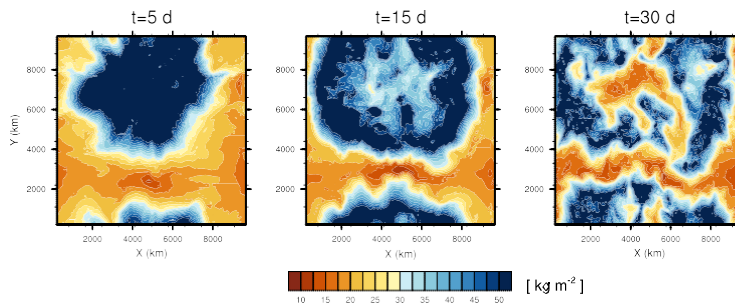
425 shows a sequence of snapshots of column water vapor from this initially aggregated exper-
 426 iment. Over a period of 30 days, the central humid region appears to collapse, becoming
 427 drier, while the surrounding moderately humid region expands as a ring before breaking up
 428 into disorganized bands. The system eventually resembles the disaggregated case in Fig. 10.
 429 The same sequence of core collapse and an expanding humid ring occurs for a variety of ini-
 430 tial conditions, including initializing with only the water vapor taken from the aggregated
 431 case and other fields horizontally uniform (not shown). In each case, the model is unable to
 432 maintain the initial aggregated cluster.

435 **6 A scale-limiting mechanism**

436 Inspired by recent studies, we seek an explanation for the apparent horizontal scale
 437 limit using the boundary layer momentum balance. The importance of the boundary layer
 438 was suggested by *Wing and Cronin* [2016], who proposed that aggregation horizontal scale
 439 was linked to the boundary layer moisture recharge time scale, and again by *Yang* [2017],
 440 who derived a general constraint on the temperature dependence of aggregation size in a 2D
 441 domain. Yang argued that boundary layer flow requires a horizontal pressure gradient to bal-
 442 ance momentum loss through the surface, an idea we apply below.



420 **Figure 10.** Snapshots of column water vapor in simulations with 55 km grid spacing and varying domain
 421 size.



433 **Figure 11.** Snapshots of column water vapor on days 5, 15, and 30 in a 9900 km domain initialized with a
 434 single aggregated cluster.

443 Here we note an additional consideration: that as the aggregation size increases, the
 444 surface windspeed increases. This can be understood through an idealized continuity equa-
 445 tion: $w_{sub} A_{sub} = u_{surf} 2\pi R_{moist}$, where w_{sub} is the subsidence rate, A_{sub} is the area of
 446 subsidence, u_{surf} is the surface wind directed into the moist region, and R_{moist} is the ra-
 447 dius of the moist region. The subsidence rate, defined as the mean pressure velocity at 500 hPa
 448 in regions of subsidence, is roughly constant with domain size, varying from 0.021 Pa/s with
 449 $L=1250$ km to 0.022 Pa/s with $L=4950$ km. This is constrained by the radiative cooling rate,
 450 which varies roughly 10% (at 500 hPa) across the three simulations, with compensating
 451 changes in static stability. Because the relative fraction of subsidence versus ascent is sim-
 452 ilarly constrained by continuity, we have $A_{sub} \propto L^2$ and $R_{moist} \propto L$, which implies that
 453 $u_{surf} \propto L$.

454 Figure 12a-c shows the surface stress vector projected on the gradient of column water
455 vapor for the three aggregating domain sizes. The stress at the moist region boundary is seen
456 to increase roughly linearly with domain size, consistent with the argument above. We sug-
457 gest that an inability to balance this increasing surface stress is the root cause of the apparent
458 upper size limit. However, the precise way in which the momentum balance fails is less clear.
459 In this model, maintaining the surface pressure gradient across an increasing distance ap-
460 pears to alter deep convection in ways that destabilize the cluster. We focus below on these
461 changes in surface pressure and convection, for which we have ready diagnostics, but future
462 work should examine the complete momentum budget in detail.

463 Surface pressure binned by column moisture is shown in Fig. 12d-f for the three do-
464 mains. As expected, each case shows a clear pressure gradient from dry to humid columns,
465 consistent with the low-level flow. The pressure difference between dry and humid regions
466 increases with domain size, sufficient to maintain a similar pressure gradient, though not to
467 singularly balance the increase in surface drag; nonlinear momentum transport therefore ap-
468 pears to be important as well. An increase in mean pressure is also visible as the domain size
469 increases, likely due to the increase in moisture content in the larger domains (Table 1).

470 *Yang* [2017] pointed out that, if the free troposphere is subject to weak horizontal pres-
471 sure gradients, and the equilibrium pressure field is hydrostatic, the boundary layer pres-
472 sure gradient will largely depend on the horizontal density gradient within the boundary
473 layer. The boundary layer density is a function of temperature and vapor pressure. The lat-
474 ter, though contributing a large fraction of the total density variation, is constrained by a
475 100% relative humidity upper bound and a 0% lower bound, which surface evaporation in
476 the dry region effectively increases. In our reference case, the boundary layer relative humid-
477 ity varies from roughly 30% to 99% (Fig. 5b), and has a comparable range in the 2640 km
478 and 4950 km cases. Boundary layer temperatures are potentially less constrained, and indeed
479 we find that boundary layer temperatures in the humid regions consistently increase with do-
480 main size (at least up to $L=4950$ km).

481 Figure 12g shows the binned temperature profiles in the 1320 km domain, and differ-
482 ences in binned temperatures between the larger domains and the 1320 km case are shown
483 in Figs. 12h,i. A warming is evident throughout the domain. In the free troposphere this
484 warming is mostly horizontally uniform, consistent with weak temperature gradient dynam-
485 ics. However, within the boundary layer the warming is concentrated in the humid regions,

486 as required to enhance the surface pressure difference. The mean temperature increase at
487 950hPa in the most humid 20% of the domain is roughly 1.2 K with $L=2640$ km and 2.1 K
488 with $L=4950$ km. As might be expected, this increase in moist static energy in the humid
489 boundary layer has a significant impact on the parameterized convection. Figure 12j-l shows
490 the binned convective mass flux, with deeper mass flux profiles in the larger domains.

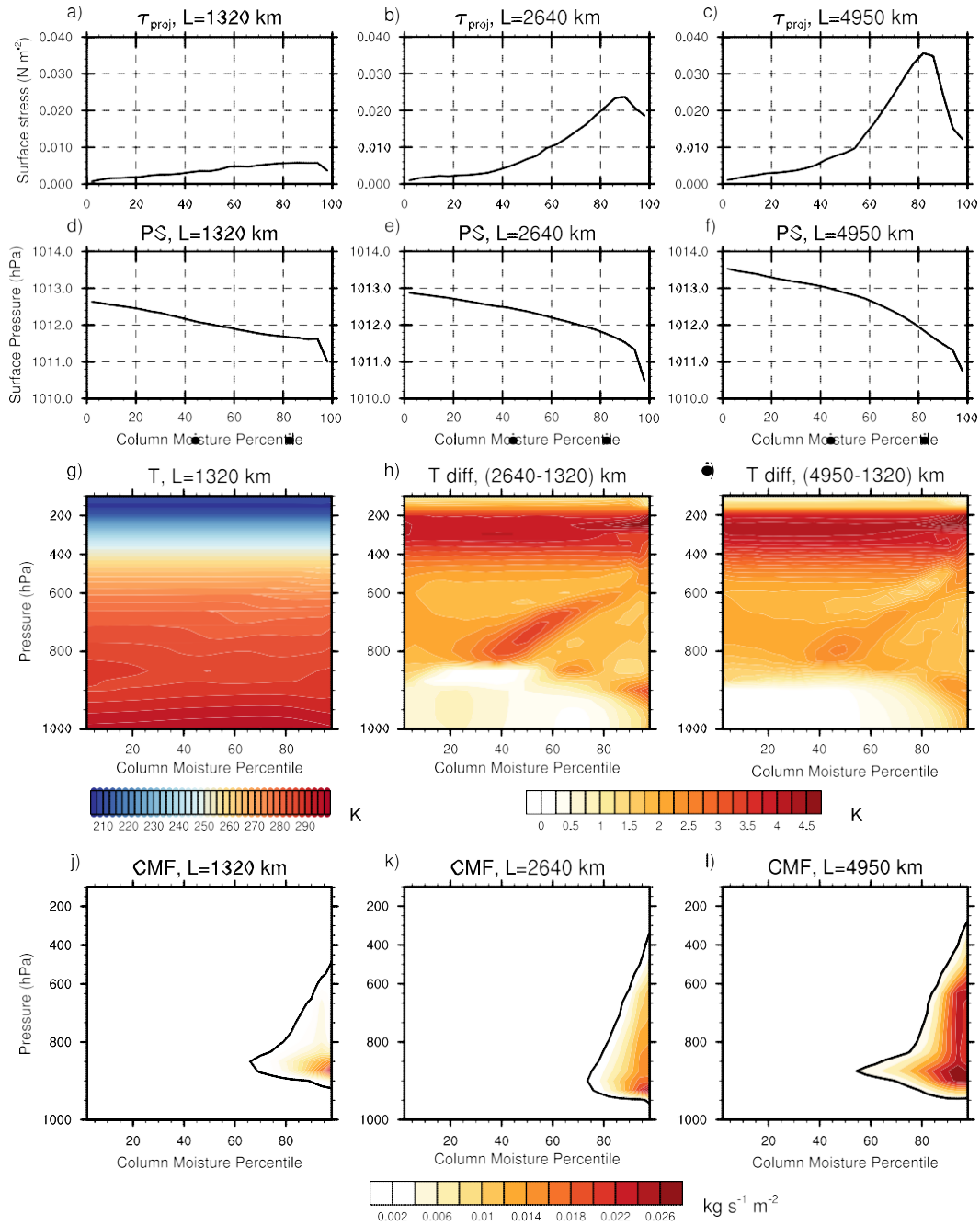
494 The deeper heating profiles from parameterized convection, in addition to increasing
495 upper tropospheric temperatures, also have a significant impact on the aggregation circula-
496 tion. The inter-CWV streamfunctions shown in Fig. 13 suggest a reason why the largest do-
497 main fails to form a robust cluster. The three smaller domains show increasingly deep large-
498 scale ascent in the humid columns, and, in the 4950 km case, a significant strengthening of
499 both the deep and shallow branches of the circulation. In general, deeper ascent is associ-
500 ated with enhanced column export of moist static energy [Back and Bretherton, 2006], and
501 requires greater diabatic input to the column in order to maintain convection. This deepening
502 circulation implies a gross moist stability that increases with the scale of aggregation.

505 **7 Summary and discussion**

506 We ran a set of convective self-aggregation simulations using the NASA GEOS AGCM
507 in a doubly periodic cartesian domain. We found that over a period of roughly 30 days, con-
508 vection became clustered in a quasi-circular humid region surrounded by dry subsidence.
509 The domain-mean humidity was reduced, and outgoing longwave radiation increased.

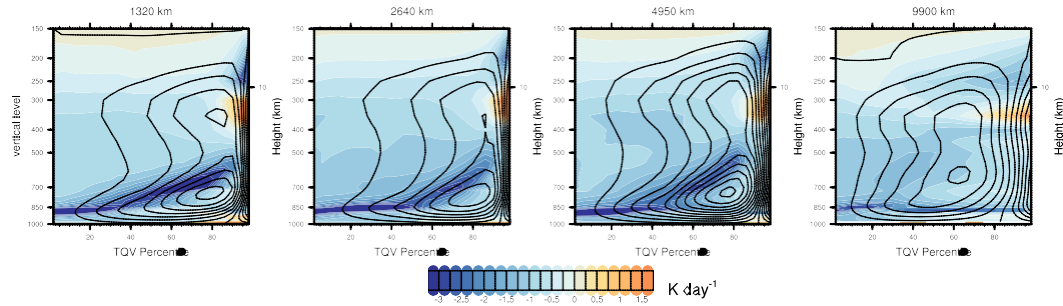
510 Aggregation has been studied in several cloud resolving models with doubly periodic
511 domains, including SAM [Bretherton *et al.*, 2005], DAM [Jeevanjee and Romps, 2013],
512 RAMS [Stephens *et al.*, 2008], UCLA-LES [Hohenegger and Stevens, 2016] as well as in
513 global AGCMs including CAM [Reed *et al.*, 2015], SP-CAM [Arnold and Randall, 2015],
514 ECHAM [Popke *et al.*, 2013], IPSL-CM5A [Coppin and Bony, 2015], ICON [Silvers *et al.*,
515 2016] and GFDL AM2 [Held *et al.*, 2007]. The range of horizontal grid spacing used here,
516 from 3 km to 110 km, and the use of an AGCM in a CRM-like domain, helps to bridge the
517 two modeling regimes. We find that the qualitative character of aggregation changes little as
518 a function of resolution, whether with convection-permitting non-hydrostatic dynamics or
519 with fully parameterized convection.

520 The column moist static energy (MSE) variance budget, developed by Wing and Emanuel
521 [2014], was used to identify processes important to aggregation. MSE variance is initially



491 **Figure 12.** (a-c) Surface stress vector projected on the gradient of column water. (d-f) Surface pressure
 492 binned by column water vapor. (g) Profiles of temperature in the 1320 km case and (h,i) temperature differ-
 493 ences relative to the 1320 km case. (j-l) Binned profiles of parameterized convective mass flux.

522 increased by longwave radiative feedbacks and, to a lesser extent, surface fluxes. As convec-
 523 tion becomes organized, the MSE variance growth rate due to the longwave term diminishes,
 524 becoming comparable in size to the shortwave feedback, while growth rates due to surface



503 **Figure 13.** Profiles of radiative cooling (shading) and stream functions representing flow between dry and
 504 humid regions (contours), in simulations with varying domain size.

525 fluxes become weakly negative. The advection terms consistently work to homogenize the
 526 MSE field, despite the development of a shallow circulation providing up-gradient MSE
 527 transport. Such a circulation has been seen in several previous studies, attributed to strong
 528 low-level radiative cooling rates in the dry region. Here the radiative cooling appears to be a
 529 clear-sky effect, which may contribute to its lack of resolution-dependence.

530 Mechanism-denial experiments, in which key physical effects are selectively removed,
 531 point again to the importance of radiative feedbacks. When longwave heating profiles were
 532 homogenized across the domain, aggregation disappeared completely. When cloud ice was
 533 removed from the longwave calculations, the aggregation weakened, with lower humidity in
 534 the ascending region. Removing cloud liquid, however, had minimal effect on the organiza-
 535 tion.

536 We also examined the role of convection-moisture interactions. Deep convection is
 537 known to be modulated by tropospheric humidity [Derbyshire *et al.*, 2004; Bretherton *et al.*,
 538 2005], and convection-moisture feedbacks are thought to play a role in the diurnal cycle of
 539 continental precipitation [Del Genio and Wu, 2010] and large-scale phenomena like the MJO
 540 [e.g., Raymond and Fuchs, 2009]. Due to our use of parameterized convection at coarser res-
 541 olutions, we were able to directly test this feedback by homogenizing the free tropospheric
 542 ($p < 850$ hPa) moisture field passed to the parameterized convection. This experiment is anal-
 543 ogous to the removal of cloud ice or liquid from the radiative calculations described above;
 544 convective tendencies are calculated as though every column had water vapor profiles equal
 545 to the domain mean. We found that removing the moisture dependence of convection re-
 546 duced the intensity of aggregation, but did not prevent the initial formation of dry regions.

547 This is consistent with the idea that initial dry patches are formed by moisture-radiative feed-
548 backs, while convection plays a role in amplifying the spatial organization.

549 Finally, we studied the scale dependence of aggregation by increasing our square do-
550 main from 1320 km to 9900 km on a side. We found that the model developed a single cir-
551 cular cluster in domains up to 5000 km, and domain-mean humidity increased with domain
552 size. In the 9900 km domain, the model developed multiple clusters, the largest of which
553 were 3-4000 km in size. We attempted to initialize the large domain with a single large clus-
554 ter, but these invariably broke apart, implying that there is an upper limit to cluster size around
555 4000 km.

556 In this case, the root cause of the upper size limit appears to be the increasing strength
557 of the low-level flow with cluster size, which results from a relatively constant fractional
558 area and rate of large-scale subsidence, both constrained by radiative cooling. The surface
559 stress in the aggregation boundary region increases roughly linearly with domain size, sug-
560 gesting that maintaining the stronger surface flow against dissipation becomes difficult for
561 larger clusters. A related factor is the maintenance of the surface pressure gradient, which re-
562 quires increasing surface pressure differences between humid and dry regions as the distance
563 between them increases. This pressure difference is partly enabled by positive temperature
564 anomalies in the humid region boundary layer, which increase with the domain size. The in-
565 creasing surface temperature leads to increased CAPE, and deeper parameterized convection.
566 The deeper convective heating leads to increasing gross moist stability at larger scales, until
567 eventually a balanced aggregated circulation becomes impossible to maintain.

568 Note that this hypothesis does not explain how the humid region boundary layer be-
569 comes warmer, only that the warmth appears to be a requirement for maintaining the surface
570 pressure gradient across a larger scale. Indeed, due to the higher near-surface temperatures,
571 surface sensible heat flux is smaller in the larger domains, and the warming by radiative flux
572 divergence within the humid-region boundary layer also decreases with domain size (not
573 shown). We find that boundary layer cooling associated with convection and water phase
574 changes does decrease, despite a small increase in rain re-evaporation, so the answer likely
575 involves the moist physics. However, the precise warming mechanism remains unclear.

576 The scale limiting mechanism suggested here is superficially similar to the wavelength
577 dependence of the gross moist stability proposed by *Kuang* [2011], although the two differ in
578 both detail and effect. *Kuang* suggested that the tropospheric temperature anomalies required

579 to drive a large-scale circulation would become larger at longer wavelengths, reducing CAPE
580 in regions of ascent and producing a shallower convective heating profile. In contrast, the
581 mechanism proposed here focuses on maintenance of the boundary layer flow [Yang, 2017],
582 with temperature anomalies required in the boundary layer rather than the free troposphere,
583 and predicts deeper convective heating in the ascent regions.

584 In nature and more Earth-like simulations, the spectrum of convective cluster sizes is
585 likely governed by a combination of processes which vary in influence depending on the
586 conditions. Other proposed scale-selecting mechanisms include the horizontal spread of high
587 clouds [Adames and Kim, 2016], the remoistening timescale of the boundary layer [Wing and
588 Cronin, 2016], the horizontal mixing of moisture [Craig and Mack, 2013], and the timescale
589 of free tropospheric moisture variability [Grabowski and Moncrieff, 2004]. The mechanism
590 identified here may act to limit the ultimate size of convective clusters which are organized
591 by other processes.

592 There is evidence from numerical simulations that aggregation scale and structure de-
593 pend on myriad factors, including surface temperature, whether SST is interactive, and de-
594 tails of the model physics. This study should be considered a snapshot of aggregation dy-
595 namics at a particular SST, with a particular model. That aggregation will develop out of
596 RCE conditions in models with such a range of physics options suggests that some tendency
597 to aggregate is likely present in nature, although obscured by the complexity of real-world
598 phenomena operating on shorter timescales. Nevertheless, many of the attributes of aggre-
599 gation - a decrease in area-mean water vapor, an increase in OLR - have been found corre-
600 lated with convective organization in real-world observations [Tobin *et al.*, 2012, 2013]. Fu-
601 ture work, perhaps under the auspices of a recently proposed RCE model inter-comparison
602 project [Wing *et al.*, 2017b], is needed to understand which aspects of aggregation are model
603 dependent and which aspects apply to nature.

607 **Acknowledgments**

608 We thank two anonymous reviewers for comments which substantially improved this manuscript.
609 This work was supported by Goddard Earth Sciences Technology And Research (GESTAR)
610 and NASA's Modeling, Analysis and Prediction (MAP) program. Computing was supported
611 by the NASA Center for Climate Simulation (NCCS). The data and software used to produce
612 all figures are archived and available by request.

604 **Table 1.** Horizontal grid size, dx , domain edge length, L , and domain mean precipitation, column water
605 vapor, outgoing longwave radiation, and net downward shortwave radiation. Averages taken over the last 30
606 days of each simulation.

Case	dx (km)	L (km)	Precip (mm/day)	CWV (mm)	OLR (W m^{-2})	Net SW (W m^{-2})
Reference	55.0	1320	3.07	25.45	284.5	360.2
uni LW	55.0	1320	1.56	35.11	226.7	149.7
no ice LW	55.0	1320	3.08	23.83	290.8	352.8
no liq LW	55.0	1320	3.13	24.67	291.5	368.1
uni QV	55.0	1320	2.59	26.96	275.2	353.0
3 km	3.7	1320	3.14	23.20	292.3	375.2
7 km	7.3	1320	3.20	22.80	287.6	374.9
14 km	14.7	1320	3.20	24.36	287.5	358.2
27.5 km	27.5	1320	3.10	24.43	290.6	366.3
110 km	110.0	1320	2.86	25.94	284.5	360.7
2640 km	55.0	2640	3.56	27.63	293.8	368.0
4950 km	55.0	4950	3.60	32.35	289.2	354.9
9900 km	55.0	9900	3.66	33.00	286.5	355.8

References

- Abbot, D. S. (2014), Resolved Snowball Earth Clouds, *J. Climate*, *27*, 4391–4402.
- Adames, A. F. and D. Kim (2016), The MJO as a Dispersive, Convectively Coupled Moisture Wave: Theory and Observations, *J. Atmos. Sci.*, *73*, 913–941.
- Andersen, J. A., and Z. Kuang (2012), Moist Static Energy Budget of MJO-like Disturbances in the Atmosphere of a Zonally Symmetric Aquaplanet, *J. Climate*, *25*, 2782–2804.
- Arnold, N. P., Z. Kuang, and E. Tziperman (2013), Enhanced MJO-like Variability at High SST, *J. Climate*, *26*, 988–1001.
- Arnold, N. P. and D. A. Randall (2015), Global-scale convective aggregation: Implications for the Madden-Julian Oscillation, *J. Adv. Model. Earth Syst.*, *7*, 1499–1518.
- Arnold, N. P., M. Branson, Z. Kuang, D. A. Randall, and E. Tziperman (2015), MJO Intensification with Warming in the Superparameterized CESM, *J. Climate*, *28*, 2706–2724.
- Bacmeister, J. T., M. J. Suarez, F. R. Robertson (2006), Rain reevaporation, boundary layer-convection interactions, and Pacific rainfall patterns in an AGCM, *J. Atmos. Sci.*, *63*, 3383–3403.
- Bony, S., B. Stevens, D. M. W. Frierson, C. Jakob, M. Kageyama, R. Pincus, T. G. Shepherd, S. C. Sherwood, A. P. Siebesma, A. H. Sobel, M. Watanabe, and M. J. Webb (2015), Clouds, circulation and climate sensitivity, *Nature geosci.*, *261–268*.
- Bretherton, C. S., P. N. Blossey, and M. Khairoutdinov (2005), An Energy-Balance Analysis of Deep Convective Self-Aggregation above Uniform SST, *J. Atmos. Sci.*, *62*, 4273–4292.
- Bony, S., and K. A. Emanuel (2005), On the Role of Moist Processes in Tropical Intraseasonal Variability: Cloud-Radiation and Moisture-Convection Feedbacks, *J. Atmos. Sci.*, *62*, 2770–2789.
- Bosilovich, M. G., R. Lucchesi, and M. Suarez (2015), MERRA-2: File Specification. GMAO Office Note No. 9 (Version 1.0), 73 pp.
- Bony, S., B. Stevens, D. Coppin, T. Becker, K. A. Reed, A. Voigt, B. Medeiros (2016), Thermodynamic control of anvil cloud amount, *Proc. Natl. Acad. Sci.*, *113*(32), 8927–8932.
- Bretherton, C. S., M. E. Peters, and L. E. Back (2004), Relationships between Water Vapor Path and Precipitation over the Tropical Oceans, *J. Climate*, *17*, 1517–1528.
- Back, L. E., and C. S. Bretherton (2006), Geographic variability in the export of moist static energy and vertical motion profiles in the tropical Pacific, *Geophys. Res. Lett.*, *33*, L17810.

644 Chou, M.-D. (1990), Parameterizations for the absorption of solar radiation by O₂ and CO₂
645 with applications to climate studies, *J. Climate*, 3, 209–217.

646 Chou, M.-D. (1992), A solar radiation model for use in climate studies, *J. Atmos. Sci.*, 49,
647 762–772.

648 Chou, M.-D. and M. J. Suarez (1994), An efficient thermal infrared radiation parameteri-
649 zation for use in general circulation models, NASA Tech. Memorandum 104606-Vol. 3,
650 NASA, Goddard Space Flight Center, Greenbelt, MD.

651 Coppin, D., and S. Bony (2015), Physical mechanisms controlling the initiation of convective
652 self-aggregation in a General Circulation Model, *J. Adv. Model. Earth Syst.*, 7, 2060–
653 2078.

654 Craig, G. C., and J. M. Mack (2013), A coarsening model for self-organization of tropical
655 convection, *J. Geophys. Res. Atmos.*, 118, 8761–8769.

656 Holloway, C. E., and S. J. Woolnough (2016), The sensitivity of convective aggregation
657 to diabatic processes in idealized radiative-convective equilibrium simulations, *J. Adv.
658 Model. Earth Syst.*, 8, 166–195.

659 Del Genio, A. D., and J. Wu (2010), The Role of Entrainment in the Diurnal Cycle of Conti-
660 nental Convection, *J. Climate*, 23, 2722–2738.

661 Derbyshire, S., I. Beau, P. Bechtold, J.-Y. Grandpeix, J.-M. Piriou, J.-L. Redelsperger, and
662 P. Soares (2004), Sensitivity of moist convection to environmental humidity, *Quart. J.
663 Roy. Met. Soc.*, 130(604), 3055–3079.

664 Emanuel, K., A. A. Wing and E. M. Vincent (2014), Radiative-convective instability, *J. Adv.
665 Model. Earth Syst.*, 6, 75–90.

666 Fuchs, Z., and D. J. Raymond (2002), Large-Scale Modes of a Nonrotating Atmosphere with
667 Water Vapor and Cloud-Radiation Feedbacks, *J. Atmos. Sci.*, 59, 1669–1679.

668 Fuchs, Z., and D. J. Raymond (2005), Large-Scale Modes of a Rotating Atmosphere with
669 Radiative-Convective Instability and WISHE, *J. Atmos. Sci.*, 62, 4084–4094.

670 Grabowski, W. W., and M. W. Moncrieff (2004), Moisture-convection feedback in the trop-
671 ics, *Q. J. R. Meteorol. Soc.*, 130, 3081–3104.

672 Grell, G. A., and S. R. Freitas (2013), A scale and aerosol aware stochastic convective pa-
673 rameterization for weather and air quality modeling, *Atmos. Chem. Phys. Discuss.*, 13,
674 23845–23893.

675 Ham, Y.-G., M. M. Rienecker, M. J. Suarez, Y. Vikhliav, B. Zhao, J. Marshak, G. Vernieres,
676 and S. D. Schubert (2014), Decadal prediction skill in the GEOS-5 forecast system, *Clim.*

677 *Dyn.*, 42, 1–20.

678 Ham, Y.-G., S. D. Schubert, Y. Vihlaiev, and M. J. Suarez (2014), An assessment of the
679 ENSO forecast skill of GEOS-5 system, *Clim. Dyn.*, 43, 2415–2430.

680 Held, I. M., M. Zhao and B. Wyman (2007), Dynamic Radiative Convective Equilibria Using
681 GCM Column Physics, *J. Atmos. Sci.*, 64(228), 228–238.

682 Hohenegger, C., and B. Stevens (2016), Coupled radiative convective equilibrium simula-
683 tions with explicit and parameterized convection, *J. Adv. Model. Earth Syst.*, 8, 1468-1482.

684 Jeevanjee, N., and D. M. Romps (2011), Convective self-aggregation, cold pools, and domain
685 size, *Geophys. Res. Lett.*, 40, 994–998.

686 Khairoutdinov, M., and K. Emanuel (2010), Aggregation of convection and the regulation of
687 tropical climate, paper presented at 29th Conference on Hurricanes and Tropical Meteorol-
688 ogy, Am. Meteorol. Soc., Tucson, Ariz.

689 Kim, D., A. H. Sobel, and I.-S. Kang (2011), A mechanism denial study on the Madden-
690 Julian Oscillation, *J. Adv. Model. Earth Syst.*, 3.

691 Kuang, Z. (2011), The Wavelength Dependence of the Gross Moist Stability and the Scale
692 Selection in the Instability of Column-Integrated Moist Static Energy, *J. Atmos. Sci.*, 68,
693 61–74.

694 Lock, A. P., A. R. Brown, M. R. Bush, G. M. Martin, and R. N. B. Smith (2000), A New
695 Boundary Layer Mixing Scheme. Part I: Scheme Description and Single-Column Model
696 Tests, *Mon. Wea. Rev.*, 128, 3187–3199.

697 Louis, J.-F., M. Tiedtke and J.-F. Geleyn (1982), A short history of the PBL parameterization
698 of ECMWF, *ECMWF Workshop on Planetary Boundary Layer Parameterization*, Read-
699 ing, U.K., 59–79.

700 Mapes, B. (1993), Gregarious Tropical Convection, *J. Atmos. Sci.*, 50(13), 2026–2037.

701 Mapes, B. E. (2016), Gregarious convection and radiative feedbacks in idealized worlds, *J.*
702 *Adv. Model. Earth Syst.*, 8, 1029-1033.

703 Mauritsen, T. and B. Stevens (2015), Missing iris effect as a possible cause of muted hydro-
704 logical change and high climate sensitivity in models, *Nat. Geosci.*, 8, 346–351.

705 Molod, A., L. Takacs, M. Suarez, J. Bacmeister, I.-S. Song, and A. Eichmann (2012), The
706 GEOS-5 Atmospheric General Circulation Model: Mean Climate and Development from
707 MERRA to Fortuna., Tech. rep., NASA/TM-2010-104606, Vol 28. NASA Technical Re-
708 port Series on Global Modeling and Assimilation, M. Suarez, Ed.

709 Moorthi, S. and M. J. Suarez (1992), Relaxed Arakawa-Schubert: A Parameterization of
710 Moist Convection for General Circulation Models, *Mon. Wea. Rev.*, *120*, 978–1002.

711 Molinari, J. and M. Dudek (1992), Parameterization of Convective Precipitation in
712 Mesoscale Numerical Models: A Critical Review, *Mon. Wea. Rev.*, *120*, 326–344.

713 Muller, C. J., and S. Bony (2015), What favors convective aggregation, and why?, *Geophys.*
714 *Res. Lett.*, *42*, 5626–5634.

715 Muller, C. J., and I. M. Held (2012), Detailed Investigation of the Self-Aggregation of Con-
716 vection in Cloud-Resolving Simulations, *J. Atmos. Sci.*, *69*, 2551–2565.

717 Nilsson, J., and K. A. Emanuel (1999), Equilibrium atmospheres of a two-column radiative-
718 convective model, *Quart. J. Roy. Met. Soc.*, *125*(558), 2239–2264.

719 Popke, D., B. Stevens, and A. Voigt (2013), Climate and climate change in a radiative-
720 convective equilibrium version of ECHAM6, *J. Adv. Model. Earth Syst.*, *5*, 1–14.

721 Putman, W. M., S.-J. Lin (2007), Finite-volume transport on various cubed-sphere grids, *J.*
722 *Comput. Phys.*, *227*(1), 55–78.

723 Putman, W., A.M. da Silva, L.E. Ott, and A. Darnenov (2014), Model Configuration for the
724 7-km GEOS-5 Nature Run, Ganymed Release (Non-hydrostatic 7 km Global Mesoscale
725 Simulation). GMAO Office Note No. 5 (Version 1.0), 18pp.

726 Putman, W. M. and M. J. Suarez (2011), Relaxed Arakawa-Schubert: A Parameterization of
727 Moist Convection for General Circulation Models, *Mon. Wea. Rev.*, *120*, 978–1002.

728 Raymond, D. J., and Z. Fuchs (2009), Moisture Modes and the Madden–Julian Oscillation, *J.*
729 *Climate*, *22*(11), 3031–3046.

730 Raymond, D. J., and X. Zeng (2000), Instability and large-scale circulations in a two-column
731 model of the tropical troposphere, *Q. J. R. Meteorol. Soc.*, *126*, 3117–3135.

732 Reed, K. A., B. Medeiros, J. T. Bacmeister, and P. H. Lauritzen (2015), Global radiative-
733 convective equilibrium in the Community Atmosphere Model 5., *J. Atmos. Sci.*, *72*, 2183–
734 2197.

735 Reed, K. A., and B. Medeiros (2016), A reduced complexity framework to bridge the gap
736 between AGCMs and cloud-resolving models, *Geophys. Res. Lett.*, *43*, 860–866.

737 Rienecker, M. M., M. J. Suarez, R. Gelaro, R. Todling, J. Bacmeister, E. Liu, M. G.
738 Bosilovich, S. D. Schubert, L. Takacs, G.-K. Kim, S. Bloom, J. Chen, D. Collins, A.
739 Conaty, A. DaSilva, W. Gu, J. Joiner, R. D. Koster, R. Lucchesi, A. Molod, T. Owens,
740 S. Pawson, P. Pegion, C. R. Redder, R. Reichle, F. R. Robertson, A. G. Ruddick, M.
741 Sienkiewicz, and J. Woollen (2011), MERRA: NASA’s Modern-Era Retrospective Analy-

742 sis for Research and Applications, *J. Climate*, 24, 3624–3648.

743 Satoh, M., K. Aramaki, and M. Sawada (2016), Structure of Tropical Convective Systems
744 in Aqua-Planet Experiments: Radiative-Convective Equilibrium Versus the Earth-Like
745 Experiment, *SOLA*, 12, 220–224.

746 Shi, X., and C. S. Bretherton (2014), Large-scale character of an atmosphere in rotating
747 radiative-convective equilibrium, *J. Adv. Model. Earth Syst.*, 6.

748 Silvers, L. G., B. Stevens, T. Mauritzen, and M. Georgetta (2016), Radiative convective equi-
749 librium as a framework for studying the interaction between convection and its large-scale
750 environment, *J. Adv. Model. Earth Syst.*, 8, 1330-1344.

751 Sobel, A. H., and C. S. Bretherton (2000), Modeling Tropical Precipitation in a Single Col-
752 umn, *J. Climate*, 13, 4378–4392.

753 Sobel, A. H., J. Nilsson, and L. M. Polvani (2001), The Weak Temperature Gradient Approx-
754 imation and Balanced Tropical Moisture Waves, *J. Atmos. Sci.*, 58, 3650–3665.

755 Sobel, A. H., G. Bellon, and J. Bacmeister (2007), Multiple equilibria in a single-column
756 model of the tropical atmosphere, *Geophys. Res. Lett.*, 34.

757 Sobel, A. H., E. Maloney (2012), An Idealized Semi-Empirical Framework for Modeling the
758 Madden-Julian Oscillation, *J. Atmos. Sci.*, 69, 1691–1705.

759 Stein, T. H. M., C. E. Holloway, I. Tobin, and S. Bony (2017), Observed Relationships be-
760 tween Cloud Vertical Structure and Convective Aggregation over Tropical Ocean, *J. Cli-
761 mate*, 30, 2187–2207.

762 Stephens, G., S. van den Heever, and L. Pakula (2008), Radiative-Convective Feedbacks in
763 Idealized States of Radiative-Convective Equilibrium, *J. Atmos. Sci.*, 65, 3899–3916.

764 Tan, J., C. Jakob, W. B. Rossow, and G. Tselioudis (2015), Increases in tropical rainfall
765 driven by changes in frequency of organized deep convection, *Nature*, 519, 451–454.

766 Thayer-Calder, K., and D. A. Randall (2009), The Role of Convective Moistening in the
767 Madden-Julian Oscillation, *J. Atmos. Sci.*, 66(11), 3297–3312.

768 Tobin, I., S. Bony, and R. Roca (2012), Observational Evidence for Relationships between
769 the Degree of Aggregation of Deep Convection, Water Vapor, Surface Fluxes, and Radia-
770 tion, *J. Climate*, 25, 6885–6904.

771 Tobin, I., S. Bony, C. E. Holloway, J.-Y. Grandpeix, G. Seze, D. Coppin, S. J. Woolnough,
772 and R. Roca (2013), Does convective aggregation need to be represented in cumulus pa-
773 rameterizations?, *J. Adv. Model. Earth Syst.*, 5, 692–703.

- 774 Tokioka, T., K. Yamazaki, A. Kitoh, and T. Ose (1988), The equatorial 30–60 day oscillation
775 and the Arakawa-Schubert penetrative cumulus parameterization, *J. Meteorol. Soc. Jpn.*,
776 *66*, 883–901.
- 777 Tompkins, A. M., and A. G. Semie (2017), Organization of tropical convection in low verti-
778 cal wind shears: Role of updraft entrainment, *J. Adv. Model. Earth Syst.*, *9*, 1046–1068.
- 779 Wing, A. A., and T. W. Cronin (2016), Self-aggregation of convection in a long channel ge-
780 ometry, *Q. J. R. Meteorol. Soc.*, doi:10.1002/qj.2628.
- 781 Wing, A. A., and K. A. Emanuel (2014), Physical mechanisms controlling self-aggregation
782 of convection in idealized numerical modeling simulations, *J. Adv. Model. Earth Syst.*, *6*,
783 59–74.
- 784 Wing, A. A., S. J. Camargo, and A. H. Sobel (2016), Role of Radiative–Convective Feed-
785 backs in Spontaneous Tropical Cyclogenesis in Idealized Numerical Simulations, *J. At-
786 mos. Sci.*, *73*, 2633–2642.
- 787 Wing, A. A., and K. A. Emanuel and C. E. Holloway and C. Muller (2017), Convective Self-
788 Aggregation in Numerical Simulations: A Review, *Surv. Geophys.*.
- 789 Wing, A. A., and K. A. Reed and M. Satoh and B. Stevens and S. Bony and T. Ohno (2017),
790 Radiative–Convective Equilibrium Model Intercomparison Project, *Geosci. Model Dev.*
791 *Discuss.*.
- 792 Yang, D. (2017), Boundary Layer Height and Buoyancy Determine the Horizontal Scale of
793 Convective Self-Aggregation, *J. Atmos. Sci.*, *75*, 469–478.
- 794 Zhang, C., B. E. Mapes and B. J. Soden (2003), Bimodality in tropical water vapour,
795 *Q. J. R. Meteorol. Soc.*, *129*, 2847–2866.